Spin- and angle-resolved photoemission study of chemisorbed $p(1 \times 1)$ O on epitaxial ultrathin Fe/W(001) films

R. L. Fink, G. A. Mulhollan, A. B. Andrews, and J. L. Erskine

Department of Physics, University of Texas at Austin, Austin, Texas 78712

G. K. Walters

Department of Physics and the Rice Quantum Institute, Rice University, Houston, Texas 77251

Chemisorbed $p(1 \times 1)$ oxygen on ultrathin epitaxial Fe films grown on W(001) are studied using spin- and angle-resolved photoemission. In agreement with theoretical predictions, single-monolayer (ML) Fe films on W(001) are found to be nonmagnetic; 2-ML-thick Fe films are magnetic, and chemisorbed $p(1 \times 1)$ oxygen does not destroy the magnetism. Even- and odd-symmetry oxygen 2p-derived bands are measured along the $\bar{\Gamma}$-$\bar{X}$ and $\bar{\Gamma}$-$\bar{M}$ directions of the two-dimensional Brillouin zone. Oxygen-derived features in the photoemission spectra exhibit magnetic exchange splitting as well as spin-dependent intrinsic linewidths that are governed by lifetime effects and initial-state mixing with Fe bands. Oxygen 2p-band narrowing resulting from the expanded Fe thin-film lattice constant is observed. The results are compared with relevant calculations and corresponding experimental studies of $p(1 \times 1)$ oxygen on bulk Fe(001) surfaces.

I. INTRODUCTION

Chemisorption at metal surfaces is an important and well-studied phenomenon. Scientific interest in atomic and molecular processes at metal surfaces is driven not only by the broad technological implications of surface chemical effects, but also by the opportunities chemisorbed atoms provide for exploring fundamental physical processes at surfaces. Relevant issues include the relationship between atomic level structure, substrate and adsorbate electronic properties, and chemical bonding, as well as issues related to how various properties of a chemisorbed system are manifested in experiments such as angle-resolved photoemission. When the substrate is magnetic, additional issues involving the role electron-spin polarization plays in all of the physical processes can also be addressed.

Of particular interest are metal-surface–adsorbate systems in which strong charge-transfer effects occur. Systems in which oxidation occurs represent important limiting cases. It is useful to follow the evolution of such systems from the precursor stage through complete oxidation since, in addition to yielding insight into the completely reacted systems, the low-oxygen-coverage systems themselves often exhibit interesting behavior. Thin-film systems involving ferromagnetic materials are particularly interesting because issues arising from magnetic properties, such as adsorbate-induced surface magnetic dead layers, magnetic quenching in ultrathin films, and induced magnetic behavior in chemisorbed atoms can be studied.

The present paper explores structural, electronic, and magnetic properties of oxygen chemisorbed on an ultrathin epitaxial Fe film grown on W(001). Angle-resolved photoemission spectroscopy, including spin detection in some experiments, is used to determine the electronic and magnetic properties of this system. Issues that govern the choice of materials used for the film and substrate are discussed in the following section, which addresses experimental procedures and film characterization. The remainder of this introductory section outlines briefly the results of a few previous studies of ordered oxygen overlayers at metal surfaces, which are closely related to material presented in this paper.

Opportunities for exploiting angle-resolved photoemission in studying ordered chemisorbed layers on metal surfaces were pointed out by Liebsch[1,2] over a decade ago. These papers examine the electronic properties of chemisorbed $c(2 \times 2)$ O and $p(1 \times 1)$ O on a Ni(110) surface based on relatively simple parametrized calculations of the ground-state electronic structure coupled with a scheme for evaluating photocurrents. The calculations included all essential parameters required to examine the utility of angle-resolved photoemission for probing adsorbate bands, including orbital symmetry, polarization dependences, and substrate electronic properties. The following features were observed: (a) the oxygen 2p valence levels exhibited dispersion and splitting resulting from adatom-adatom interactions, a property that is readily observed as electron wave vector (k) dependence of corresponding peaks in photoemission spectra, (b) the adsorbate resonances are broadened and split because of hybridization with substrate conduction bands, a property also evident in the width of photoemission peaks, (c) orbital-symmetry effects play a principal role in determining the incident light-polarization dependences exhibited by the resonances, and (d) final-state effects play a significant role in the photoelectron cross sections. These particular calculations did not deal with the possibility of magnetic splitting of the oxygen states induced by the

magnetic substrate, but subsequent theoretical work[3] and recent experiments,[4-6] including the present work, has shown that magnetic properties play an important role in determining the energy levels and intrinsic photoemission linewidths associated with chemisorbed atoms.

All of the effects predicted theoretically have been subsequently verified by experiment. DiDio, Plummer, and Graham[7] carried out angle-resolved photoemission studies of momentum-dependent line shapes in the $c(2\times2)$ O on Ni(110) system. These experiments showed that variation of photoemission line shapes with $\mathbf{k}$ can be accounted for in terms of hybridization of the energy bands of the two-dimensional overlayer with those of the three-dimensional solid. A corresponding study by Panzner, Mueller, and Rhodin[8] of $p(1\times1)$ S on Fe(001) tested essential predictions involving orbital symmetry, polarization dependences, and selection rules. Some of the conclusions reached by these studies merit reexamination in view of the significant magnetic effects, in particular the magnetic exchange splitting of oxygen $2p$ orbitals, which have been recently observed by spin-sensitive experiments.[4-6]

More recent angle-resolved photoemission studies which include the detection of electron spin have begun to explore these effects at surfaces of bulk magnetic systems and to expand the issues addressed to include electron-spin and exchange effects. Those studies show that the orbital levels of $p(1\times1)$ O and $c(2\times2)$ S on bulk Fe(001) exhibit $k_{\parallel}$-dependent exchange splitting and linewidths that are functions of both orbital symmetry and spin. Similar effects[9] have been observed at the surface of Ni(110) prior to the formation of NiO. The present paper extends the above cited work by exploring the same issues for ordered adsorbates on ultrathin epitaxial magnetic films. In addition, another issue relevant to thin-film systems has been raised: Can ferromagnetism exist in thin-film systems following the charge transfer accompanying chemisorption?

II. EXPERIMENTAL CONSIDERATIONS

Our choice of W(001) as a substrate material was based on several requirements of the film-substrate system. The most important requirement was that the system must exhibit excellent epitaxy at one to two monolayer (ML) thicknesses while also maintaining a magnetic state at accessible temperatures. Film-substrate systems [such as Fe on Ag(100)], which may not achieve good epitaxy conditions until many layers have been grown,[10] are less desirable because their electronic behavior will not be two dimensional. It is also desirable that the film lattice be expanded over the bulk value. The accompanying increase in magnetic strength of the film should help compensate for the decrease in surface magnetic moments that generally accompanies oxygen adsorption as well as corresponding effects due to film-substrate interactions.

All of these prerequisites are met by the Fe/W(001) system. Our magneto-optic Kerr-effect studies[11] of $p(1\times1)$ Fe on W(001) have shown that films greater than 1 ML are ferromagnetic with Curie temperatures slightly above 300 K (for a 1.5-ML-thick film) and that a $p(1\times1)$

O layer on a 2-ML film does not quench the magnetism. In addition, despite the significant strain resulting from the mismatch between bulk Fe and W lattice constants ($\approx9.5\%$), the epitaxy of Fe on W(001) is very good for 1-2-ML-thick films.

The angle-resolved photoemission experiments reported here were carried out at the National Synchrotron Light Source (NSLS), Brookhaven National Laboratory. Spin- and angle-resolved measurements were conducted using the U5U beam line[12] with a total energy resolution (monochromator and photoemission analyzer) of 300 meV and angular resolution of $\pm1.5°$. Spectrometer limitations enabled probing spin-polarized states of even symmetry only. The thin magnetic films were magnetized by application of a high-current pulse to coils near the sample having an axis along a $\langle11\rangle$ crystal direction. The 2-ML Fe films exhibit square magnetization loops (remanent magnetization along $\langle11\rangle$ when $H=0$), suggesting that either the film is magnetically isotropic or has an easy axis of magnetization along the $\langle11\rangle$ direction. Although the Curie temperature of a 1.5-ML Fe film on W(001) is approximately 320 K, the films were cooled to 110 K for all spin-polarized electron experiments prior to data acquisition. Angle-resolved photoemission data without spin detection was acquired on the U16A beam line, also at NSLS, using a combined energy resolution of 140 meV and angular resolution of $\pm1°$. Initial states of both odd and even symmetry were accessible at U16A. In the non-spin-polarized studies, all experimental data were acquired with the sample at 300 K and with no effort to magnetically align the thin Fe films.

The 1-cm-diam by 1-mm-thick W(001) disks were oriented by x-ray Laue techniques and prepared by spark cutting followed by mechanical polishing with diamond paste. Angular orientation of the crystal (001) axis relative to its surface normal was judged to be within $\pm5°$ based on Laue photographs taken while cutting the crystal. This value was subsequently confirmed by observing low-energy electron-diffraction (LEED) spot profiles. The W(001) surface was cleaned using conventional methods (repeated annealing at 1300 °C in oxygen followed by flashing to 2200 °C. Surface conditions were checked by LEED [including the observation of the $c(2\times2)$ phase, which occurs on clean W(001) below 280 K], and surface contamination was monitored by Auger spectroscopy (carbon and oxygen) and photoemission. Generally, the total surface impurity concentration prior to film growth was below 2% and consisted mostly of trace amounts of carbon.

Epitaxial Fe films were prepared by electron-beam evaporation from the tip of a high-purity Fe wire. Growth rates of ~1 Å/min were employed. The best epitaxy, as judged by the quality of LEED patterns (the sharpness of spots and low diffuse background) was generally achieved with the W(001) substrate held at ~1000 K during deposition of the first layer and at 300 K or below for the second and additional layers. An extensive account of magnetic behavior, film-growth properties, and structure of $p(1\times1)$ Fe on W(001) is in preparation and is planned to be reported in the future.[11] We have carried out extensive LEED I-V and spot-profile-analysis studies, as well

as x-ray and Auger electron forward-scattering analysis of Fe films grown on W(001). For purposes of the present discussion, it is sufficient to state that 1- and 2-ML-thick Fe films on W(001) yield excellent LEED patterns and exhibit very good epitaxy. LEED spot diameters for 1- and 2-ML films on W(001) are similar to those observed for the best clean W(001) surfaces, suggesting the absence of strain-relieving dislocations in the Fe films.

Oxygen doses were accomplished by admitting high-purity gas through a Varian variable leak value without a directional doser. Oxygen exposures were determined from gauge readings of a standard UHV-24 nude ion-gauge tube (uncorrected for oxygen) at pressures of $\sim 1 \times 10^{-8}$ Torr. LEED patterns of the oxygen-dosed Fe layer were generally of poorer quality compared with those of the clean films, but maintained an unmistakable $p(1 \times 1)$ symmetry. The larger LEED spot size and increased diffuse background at saturated (1 ML) oxygen coverage suggest that the $p(1 \times 1)$ O layer has a significant degree of disorder. Nevertheless, the $p(1 \times 1)$ oxygen was well ordered enough to yield good dispersion measurements of the O $2p$ levels, characteristic of an ordered oxygen overlayer. Annealing the oxygen-dosed Fe(001) surface to 900 K yielded a sharp $p(1 \times 1)$ pattern, but this procedure was also found to produce an irreversible change in the film magnetic properties; therefore, no annealing was carried out after oxygen doses in the experiments described here.

III. EXPERIMENTAL RESULTS

A. Angle-resolved photoemission without spin detection

We first present and briefly discuss results of our non-spin-resolved experiments and then present our spin-polarized photoemission results. In discussing our angle-resolved photoemission results, we will refer to experiments carried out using even- or odd-symmetry emission geometry using s- or p-polarized light, and using specific electron-emission angles which define the location of initial states in the two-dimensional Brillouin
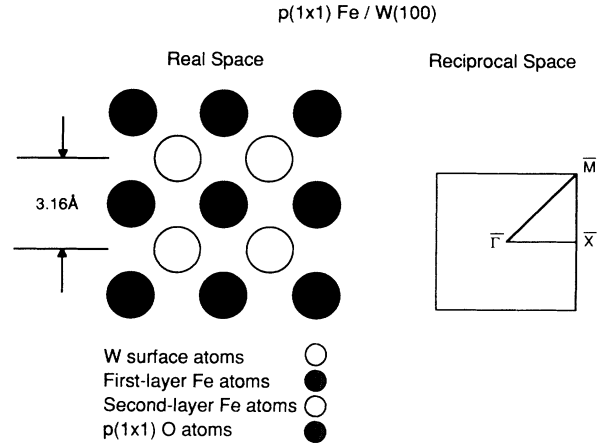

p(1x1) Fe / W(100)

FIG. 2. Real-space structure of $p(1 \times 1)$ O on 2 ML Fe/W(001) and corresponding two-dimensional Brillouin zone. The real-space structure is a view along the surface normal. Atoms of a given shading lie directly below other atoms denoted with the same shading, irrespective of species. Angle-resolved photoemission data were acquired along both in-plane high-symmetry directions with the in-plane momentum $k_{\parallel} = 0.512(E_k)^{1/2} \sin \theta_E$ ranging from $\overline{\Gamma}\text{-}\overline{X}$ (along $\langle 100 \rangle$) and $\overline{\Gamma}\text{-}\overline{M}$ (along $\langle 110 \rangle$).

zone. The conventions and definitions required to specify these parameters are presented in Figs. 1 and 2. Rotation of the crystal is permitted about either the x and y axis. An x-axis rotation yields a non-normal incidence angle and introduces a p-polarized component of the vector potential A, which specifies the polarization of incident light.

Figure 3 displays two energy-distribution curves (EDC's) for $p(1 \times 1)$ Fe on W(001) before and after exposing the Fe surface to 1.0 L (1 L $=1 \times 10^{-6}$ Torr sec) of oxygen. In conjunction with the work reported here, we have carried out extensive angle-resolved photoemission studies of clean $p(1 \times 1)$ Fe films on W(001), which are planned to be reported separately.[13] These studies have determined the prominent two-dimensional Fe bands and
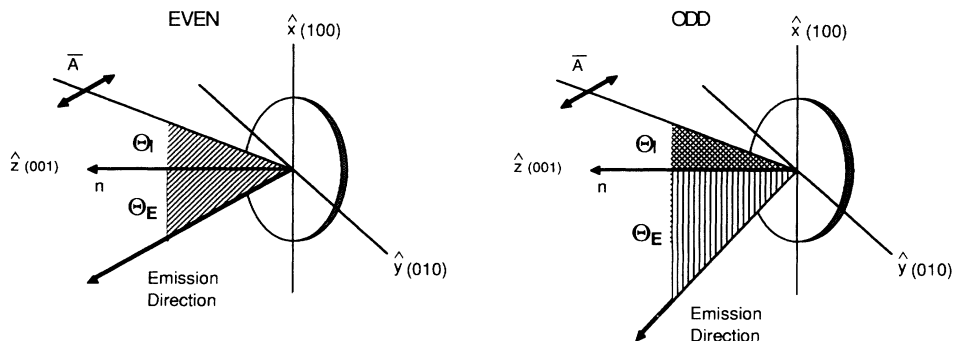

FIG. 1. Experimental geometry used in angle-resolved measurements. Light is incident on the sample at an angle θ_I with respect to the surface normal n. Electrons emitted at an angle θ_E with respect to the surface normal are collected by the analyzer. The light polarization and angle of incidence are set by rotating the sample about either the x or y axis. While electrons in both the even- and odd-state geometries are collected in a mirror plane containing the surface normal, the two geometries differ in that the vector potential A is parallel to the mirror plane in the even-state geometry and perpendicular to the mirror plane in the odd-state geometry.

projected bulk W bands that are observed at most of the photon energies and $k_\parallel$ values used in the experiments reported here. Nearly all of the prominent two-dimensional Fe bands lie within 2–3 eV of E_F (as apparent in subsequent discussions); therefore assignment of the O $2p$ levels in most of the EDC's is unambiguous. In addition, we have found that the O $2p$-band dispersion of $p(1\times1)$ O on the W(001)-supported epitaxial Fe films is very similar to corresponding bands of $p(1\times1)$ O on Ni(110) and Fe(001) bulk-metal surfaces. The polarization dependences are also similar, but there are clear differences in binding energies and bandwidths throughout the two-dimensional Brillouin zone as well as different energy dependences in the photoemission cross sections.

Returning to Fig. 3, the prominent oxygen-derived peak at 4.5 eV is consistent with a $P_{x\pm y}$ symmetry state at $\overline{\Gamma}$. Corresponding spectra (refer to the lower pair of spectra shown in Fig. 4), also taken in normal-emission

geometry with both s- and p-polarized light but at $h\nu = 40$ eV, show that there are significant photon-energy dependences in the photoelectron cross section as well as polarization dependences. The O $p_{x\pm y}$ peak is still apparent in the s-polarized spectrum at $\overline{\Gamma}$, but the cross section is clearly reduced compared with the result at $h\nu = 21$ eV. With p-polarized light and using normal-emission geometry, a second peak centered around 6.5 eV is apparent in the spectra of Fig. 4. This peak will later be shown to result from an exchange-split O p_z state.

The upper two EDC's of Fig. 4 were taken at $k_\parallel = \overline{M}$ in even-symmetry geometry at two incident angles. The two peaks at 5.0 and 6.5 eV exhibit polarization sensitivity consistent with assignment of the lower peak (5.0 eV) to a p_z character state and the upper peak to a $p_{x\pm y}$ character state.

The peak assignments indicated in Fig. 4 suggest that the oxygen-derived states having p_z and $p_{x\pm y}$ character
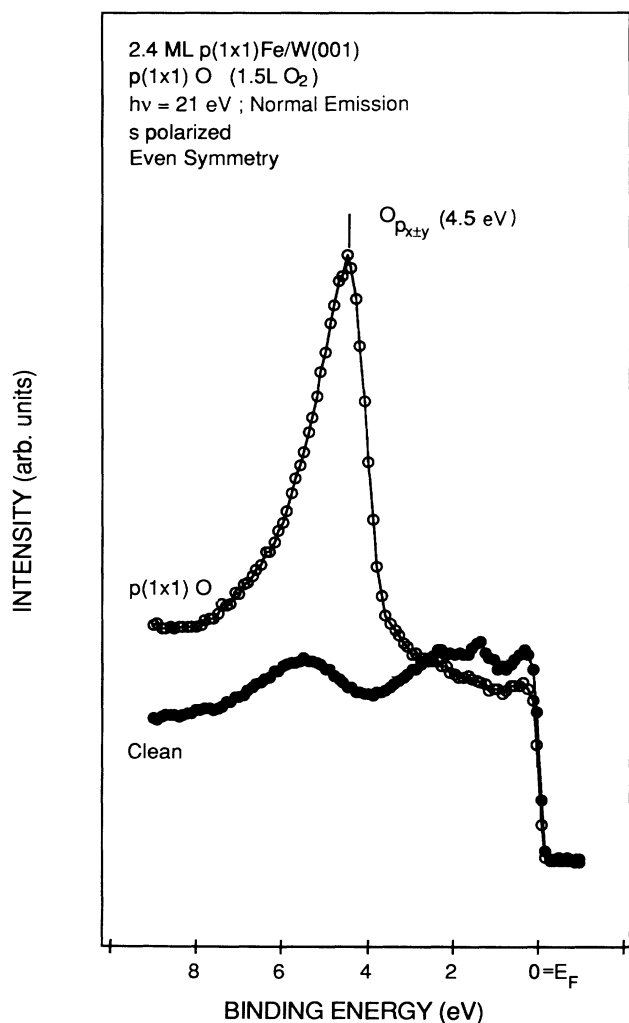

FIG. 3. Normal-emission even-symmetry angle-resolved photoemission spectra of clean (●) and oxygen-covered (○) 2.4 ML Fe/W(001) for $h\nu = 21$ eV. Emission from the oxygen $2p$ states is localized at 4.5 eV binding energy.
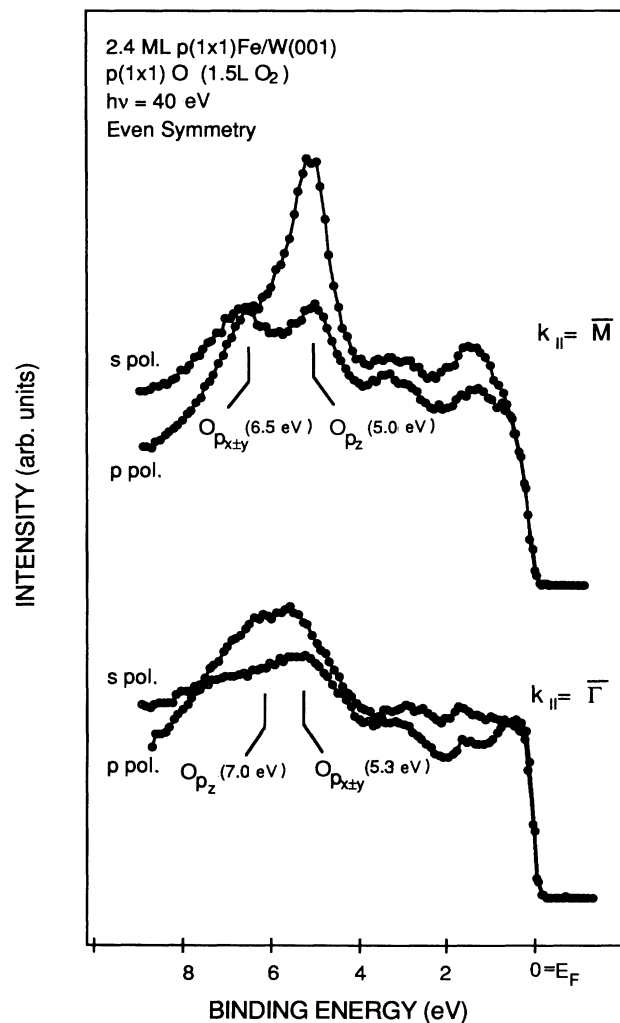
FIG. 4. Normal-emission ($\overline{\Gamma}$) and zone-edge ($\overline{M}$) even-state angle-resolved photoemission spectra of $p(1\times1)$ O on 2.4 ML Fe/W(001) for $h\nu = 40$ eV. The O p_z and $p_{x\pm y}$ states are differentiated by their response to s polarization (○) and p polarization (●).

exhibit significant dispersion along the $\bar{\Gamma}$-$\bar{M}$ direction of the two-dimensional Brillouin zone and, in fact, cross. Figure 5 displays the $k_\parallel$ dependence of the O $2p$ states along the $\bar{\Gamma}$-$\bar{X}$ and $\bar{\Gamma}$-$\bar{M}$ directions of the two-dimensional Brilouin zone obtained by numerous (non-spin-polarized) angle-resolved photoemission measurements. The photon energies and symmetry used in the various experiments are indicated in Fig. 5. Additional selected EDC's, corresponding to $k_\parallel$ along $\bar{\Gamma}$-$\bar{M}$, will be presented in conjunction with a discussion of spin-polarized data. These spectra will be followed with a discussion of the appearance of a feature at low binding energies (~ 3 eV) that appears to be an oxygen-induced spin-polarized state of the Fe surface.

If we assume (as suggested by the calculations referred to previously) that the O-O interaction is primarily responsible for the dispersion of the O $2p$ bands, the increase in lattice constant of the Fe film compared with the bulk Fe crystal should result in a reduced bandwidth for $p(1\times1)$ O on the film. This appears to generally be the case. If the widths of corresponding O $2p$ bands are compared for the thin-film and bulk Fe surfaces, the energy differences along $\bar{\Gamma}$-$\bar{X}$ or $\bar{\Gamma}$-$\bar{M}$ of the two-dimensional Brillouin zone are typically less for the film. Specifically, the bandwidth of the $p_{x\pm y}$ band along $\bar{\Gamma}$-$\bar{M}$ for oxygen on bulk Fe is approximately 2.2 eV, whereas the corresponding value for the thin film is approximately 1.3 eV. Some caution is in order in making this comparison because of

the apparent disagreements between the spin-polarized[5] and non-spin-polarized results[8] which lie beyond the cited experimental error.

B. Spin- and angle-resolved photoemission

Figure 6 displays spin- and angle-resolved photoemission EDC's for $p(1\times1)$ O on a 2-ML Fe film. The majority- and minority-spin EDC's were obtained using the procedure described by Clarke et al.[5] The two sets of data represent measurements taken at normal emission ($\theta_E = 0$), corresponding to $\bar{\Gamma}$ using $\theta_I = 70°$ (p polarization) and $\theta_I = 35°$ (s polarization). At the 60 eV photon energy used, emission from the $p_{x\pm y}$ states (which should be seen in both s- and p-polarized spectra) is weak. The p-polarized spectra, which emphasizes emission from p_z orbitals, clearly exhibits exchange splitting of the p_z orbital at $\bar{\Gamma}$, as shown in Fig. 6. The splitting of O p_z states at $\bar{\Gamma}$ is confirmed by corresponding measurements at $h\nu = 53$ eV.

Figures 7 and 8 display typical examples of the curve-fitting procedure used to establish the binding energies of peaks in EDC's based on s- and p-polarized spectra similar to those in Fig. 6. Beginning with the p-polarized EDC, we assume that the O p_z orbital dominates both majority- and minority-spin EDC's around 4–8 eV binding energy. We also assume that peaks from spin-split
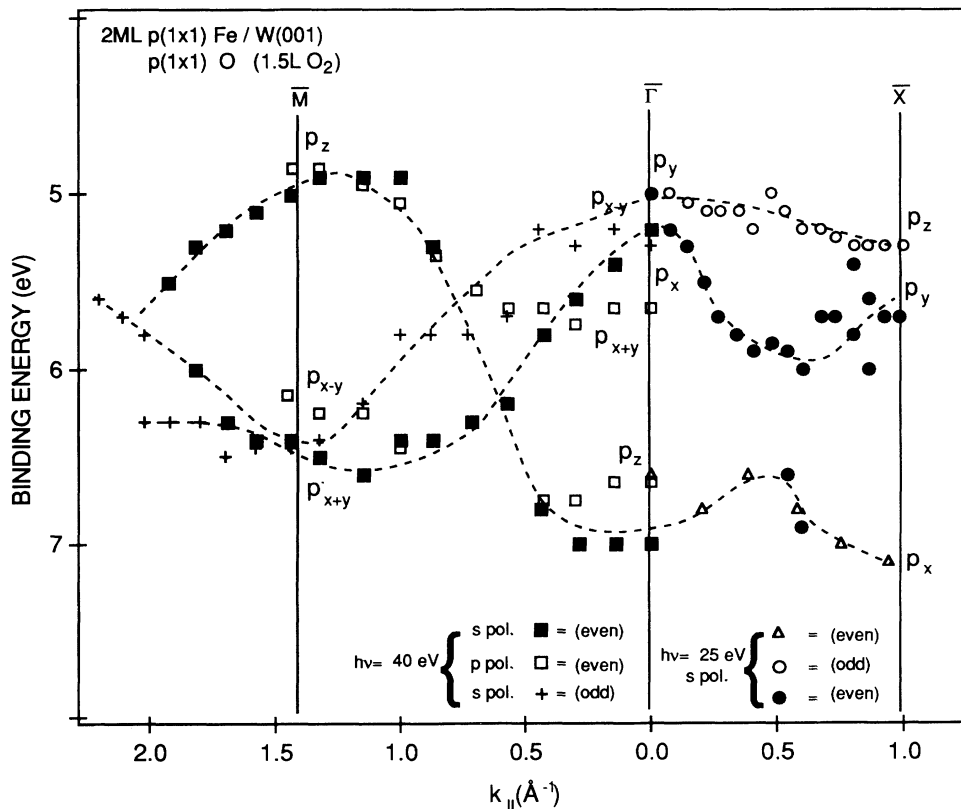

FIG. 5. Two-dimensional band structure of O $2p$ orbitals along $\bar{\Gamma}$-$\bar{M}$ and $\bar{\Gamma}$-$\bar{X}$ acquired with $h\nu = 40$ and 25 eV. Total dispersion of the $2p$ states over the Brillouin zone is ~ 2 eV.

states should have equal weights, but not necessarily the same widths. Based on these criteria and after suitable background corrections have been made, good fits to the experimental data are obtained based on Lorentzian line shapes convoluted with a fixed Gaussian profile to account for the finite resolution of the analyzer.

Table I summarizes binding energies of the various $2p$ states of $p(1\times1)$ O at three locations of the two-dimensional Brillouin zone as determined by our fits to data acquired with 2-ML $p(1\times1)$ Fe films. Also presented are corresponding results obtained by Panzner, Mueller, and Rhodin[8] for $p(1\times1)$ O on bulk Fe(001) and, for later reference, binding energies of exchange-split $2p$ O levels at $\bar{\Gamma}$ and $\bar{X}$ obtained by Clarke et al.[5] from spin-polarized photoemission studies of $p(1\times1)$ O on bulk Fe(001). The measured p_z exchange splitting at $\bar{\Gamma}$ is smaller for O on the 2-ML Fe film than on the bulk surface (1.3 eV for bulk Fe, 0.9 for the Fe film); the uncertainties in the $p_{x\pm y}$-orbital binding energies for O adsorp-

tion on the thin Fe films were too large to verify the splitting of $p_{x\pm y}$ states.

Table II presents the peak widths of O-derived peaks as a function of binding energy measured from E_F compiled from our spin-resolved data. One fact that has emerged from our spin-polarized photoemission results and similar results obtained by Clarke et al.[5] is that caution is required in attributing broadening of photoemission peaks from adsorbates on magnetic metals solely to adatom hybridization effects. Exchange effects can dominate linewidths in non-spin-resolved photoemission spectra.

C. Oxygen-induced resonances

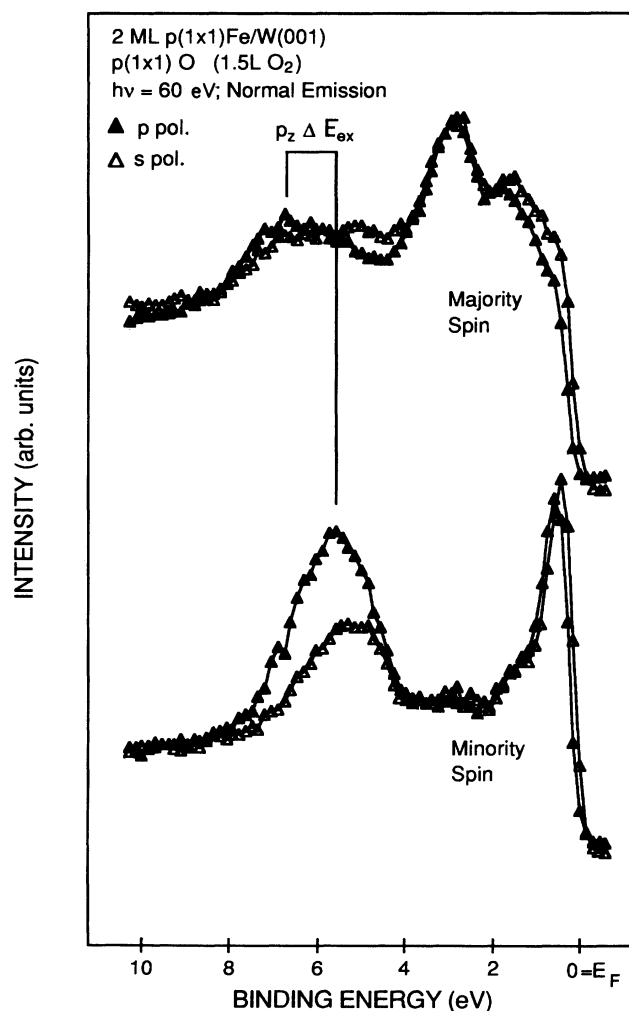The adsorption of O also leads to resonance enhancements which exist across the manifold of Fe states. These

FIG. 6. Comparison of s-polarization ($\triangle$) and p- polarization ($\bullet$) sensitivities in spin- and angle-resolved photoemission spectra using normal-emission geometry and $hv=60$ eV. The p_z- orbital exchange spilling is shown based on the p-polarization spin-resolved spectra.
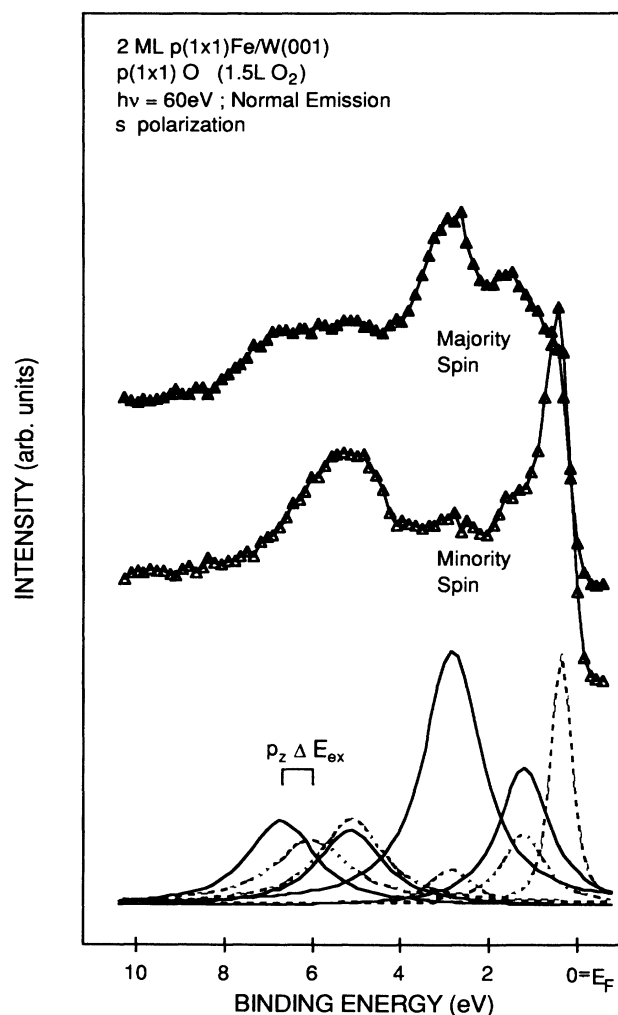

FIG. 7. Lorentzian-curve fits to s-polarization spectra of Fig. 6. While the Lorentzians are expected to be adequate representations of the O $2p$ orbitals, those Lorentzians representing features in the conduction band (from clean sample data) are inserted primarily to account for the background in the vicinity of the O states. Majority-spin features are indicated by solid lines in the fitted curves, minority-spin features by dashed lines.
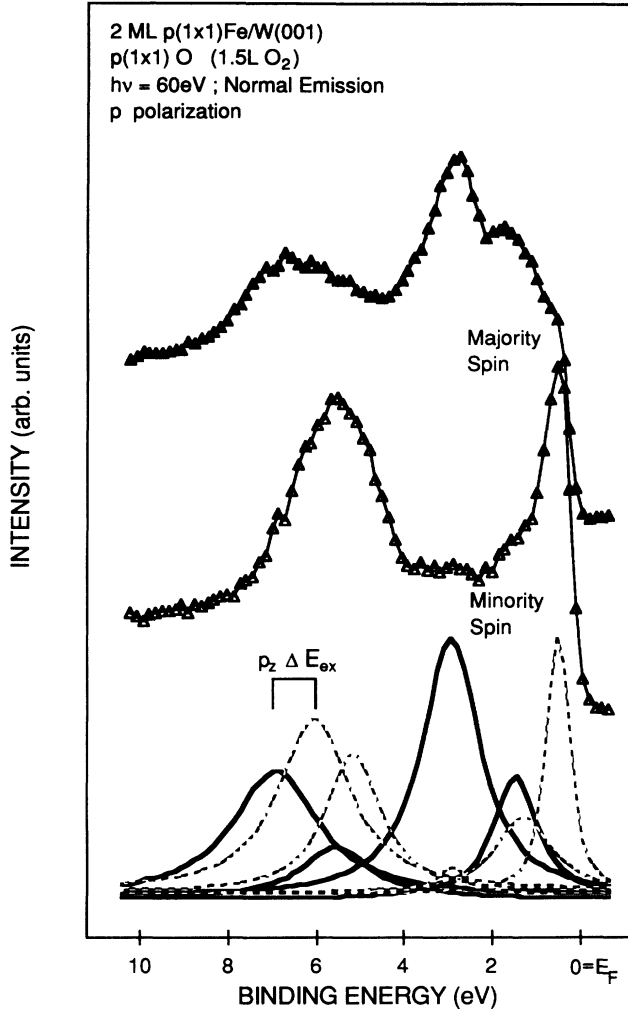
2 ML p(1x1)Fe/W(001)
p(1x1) O (1.5L O$_2$)
hv = 60eV ; Normal Emission
p polarization

Majority
Spin

Minority
Spin

P$_z$ Δ E$_{ex}$

10   8   6   4   2   0=E$_F$
BINDING ENERGY (eV)

FIG. 8. Gaussian-convoluted Lorentzian-curve fits to p-polarization spectra of Fig. 6. Majority-spin features are indicated by solid lines, minority-spin features by dashed lines.

TABLE II. Full width at half maximum (FWHM) of oxygen orbitals on 2 ML Fe/W(001) at two points in the two-dimensional Brillouin zone compared with oxygen on bulk Fe(001) as in Table I.

Symmetry point	Orbital	Film FWHM (eV)	Bulk[a] FWHM (eV)
$\overline{\Gamma}$	$p_{x \pm y}$	1.46↑±0.22	1.2↑
		0.77↓±0.30	0.7↓
	p_z	1.87↑±0.25	1.1↑
		2.15↓±0.14	2.5↓
$\overline{M}$	$p_{x \pm y}$		
	p_z	1.48↑±0.64	
		1.02↓±0.13	

[a]Reference 5.

resonance states generally yield weaker emission than the O 2p orbitals which appear as prominent peaks at binding energies greater than 4 eV. Angle-resolved hv=40 eV spectra reveal a relatively weak and nearly dispersionless enhancement near 3 eV from $\overline{\Gamma}$ to $\overline{M}$. Oxygen-induced resonances, as mapped with angle-resolved measurements, are also present along the $\overline{\Gamma}$-$\overline{X}$ direction, existing in a relatively flat band centered about 2.8 eV binding energy. The zone-center spin-resolved spectrum shown in Fig. 9, however, reveals two resonances, one in the majority-spin spectrum at 3.0 eV and much weaker one in the minority-spin spectrum at the same energy. Coverage-dependent data reveal that the resonance band near $\overline{\Gamma}$ is primarily of majority-spin character. At $\overline{M}$ (as shown in Fig. 10), two resonances are visible, a shifted majority state at 3.0 eV and a minority state at slightly lower binding energy. Here the majority-spin resonance is somewhat weaker that the minority-spin resonance.

TABLE I. Binding energies of oxygen orbitals on 2 ML Fe/W(001) at three points in the two-dimensional Brillouin zone compared with spin- and angle-resolved data acquired from the surface of bulk Fe(001). Arrows indicate majority (↑) and minority (↓) states.

Symmetry point	Orbital	Film binding energy (eV)	Bulk[a] binding energy (eV)	Bulk[b] binding energy (eV)
$\overline{\Gamma}$	$p_{x \pm y}$	5.0↑		5.0↑
		4.9↓	4.6	4.5↓
	p_z	6.6↑		7.1↑
		5.7↓	6.8	5.8↓
$\overline{M}$	$p_{x \pm y}$	6.3	6.8	
		5.1↑		
	p_z	4.9↓	5.0	
$\overline{X}$	p_x	7.1	6.8	8.6↑
				8.4↓
	p_y	5.3	5.8	
	p_z	5.7	5.6	6.4↑
				6.4↓

[a]Reference 8.
[b]Reference 5.

These resonances, as obtained by both spin-integrated angle-resolved and spin-resolved methods, are shown in Fig. 11 as a function of binding energy across the Brillouin zone with corresponding clean 2-ML Fe/W(001) data. The binding energies for the analogous states from $\bar{\Gamma}$ to $\bar{X}$ are also shown in Fig. 11.

IV. DISCUSSION

On bulk Fe(001), the $2p$ O $p_{x \pm y}$ orbitals exhibit greater dispersion than do the p_z orbitals as a result of the stronger O-O interactions. In the thin-film system, the Fe bilayer adopts the lattice constant of the W substrate such that planer Fe bond lengths are increased by 10% compared with the bulk Fe surface. This expansion results in a reduced O-orbital overlap which contributes to the observed decrease in bandwidths of the $p_{x \pm y}$ levels. In contrast, the p_z bandwidths of O on the Fe film remains near the value for the bulk Fe(001) surface. This

suggests that the vertical bond distance for the O on the film is not significantly different from the corresponding distance on the bulk Fe surface. In other words, the oxygen atoms on the strained Fe surface are not found deeper within the fourfold hollow sites than they are when adsorbed upon the bulk Fe(001) surface. LEED studies to test this hypothesis are underway. Overall, the band structure of the O on the film is very similar to that of O on bulk Fe, including the avoided crossing along $\bar{\Gamma}$-$\bar{X}$ due to mixing of the Fe $3d$ and overlayer bands.[8]

The reductions in bandwidth may also be interpreted as partially resulting from decreased interaction between the $p(1 \times 1)$ O layer and substrate. A consequence of this would be a reduced exchange splitting in the overlayer levels. Based on the spin-resolved measurements, the splittings are indeed smaller for $p(1 \times 1)$ O on 2 ML Fe. However, a recent local-spin-density-approximation (LSDA) calculation of this system predicts that O adsorption reduces by $\frac{2}{3}$ the moments in the Fe layer at the W
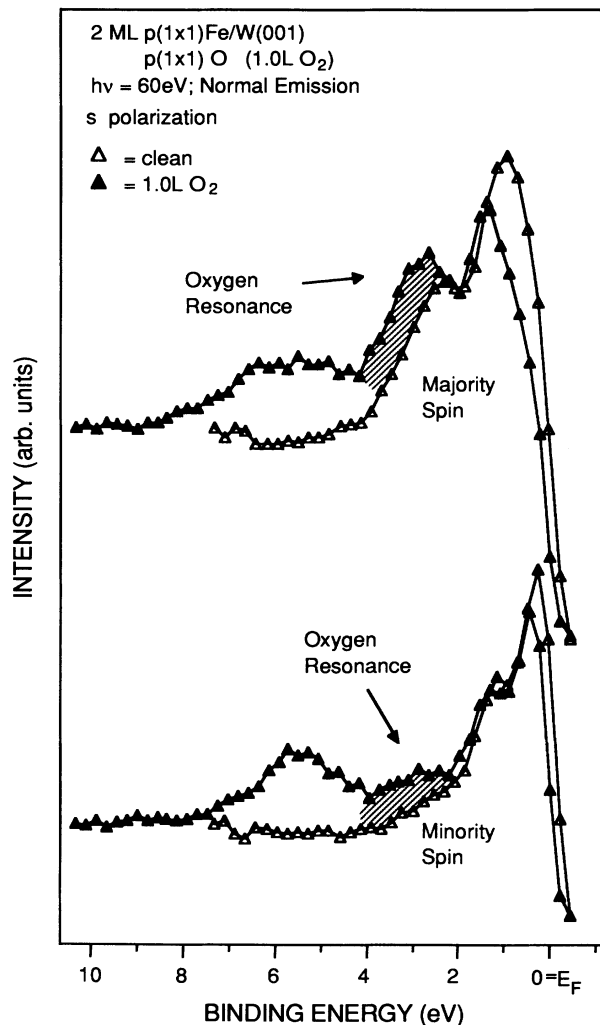

FIG. 9. Normal-emission s-polarization spin- and angle-resolved spectra of clean ($\triangle$) and $p(1 \times 1)$ O on 2 ML Fe/W(001) ($\bullet$) using $h\nu = 60$ eV. Note the locations of the peaks enhanced by the presence of oxygen.
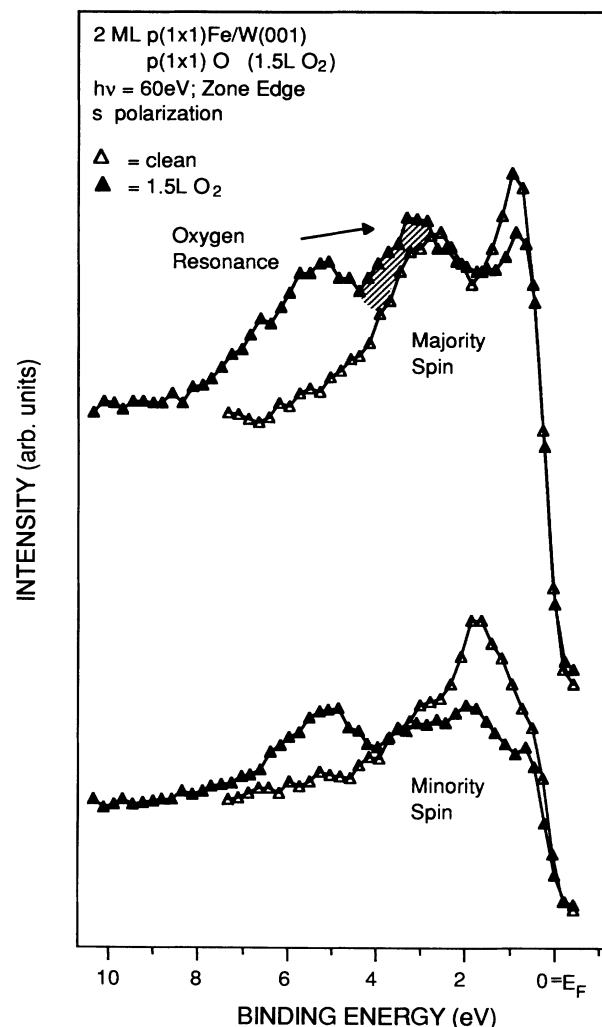
FIG. 10. Zone-edge ($\bar{M}$) s-polarization spin- and angle-resolved spectra of clean ($\triangle$) and $p(1 \times 1)$ O on 2 ML Fe/W(001) ($\bullet$) using $h\nu = 60$ eV. Note the locations of the oxygen-enhanced peaks.
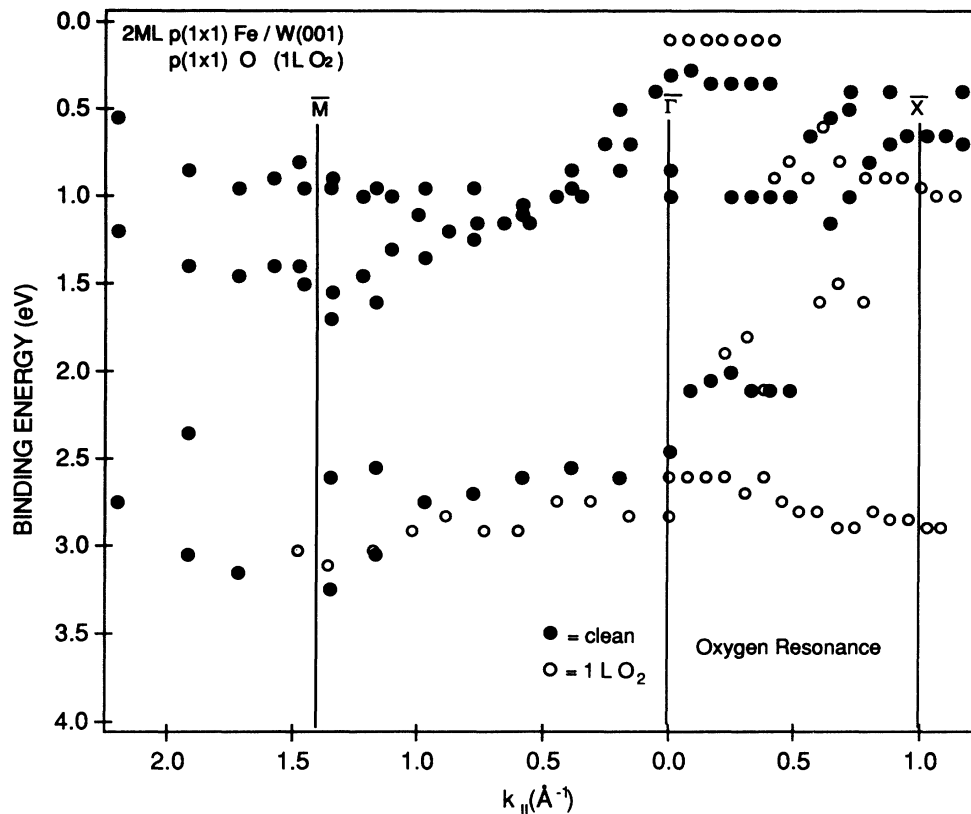
FIG. 11. Two-dimensional band structure of pure Fe states and O resonances along $\overline{\Gamma}$-$\overline{M}$ and $\overline{\Gamma}$-$\overline{X}$.

interface while leaving the upper layer virtually unchanged.[14] This result implies a reduced exchange splitting in the p_z orbitals, while possibly leaving the $p_{x\pm y}$-orbital exchange splitting intact if the Fe d_{xy} orbitals responsible for the exchange splitting are those localized in the upper Fe layer. Therefore it is not possible at this time to determine unambiguously whether the reduced exchange splitting in the $p_{x\pm y}$ orbitals is primarily a lattice expansion or diminished substrate-overlayer interaction effect.

In general, line shapes characteristic of photoemission are determined by a combination of intrinsic lifetime effects, such as hole decay via Auger deexcitation, and many-body effects, e.g., electron-hole pair excitations. Only under certain conditions is it possible to identify the isolated contribution of a single effect. The linewidth of the O orbitals is determined exclusively by intrinsic effects when contributions from the Fe film are suppressed. This occurs when either hybridization with the Fe is forbidden by symmetry, as it is for the $p_{x\pm y}$ states at $\overline{\Gamma}$, or when the orbitals lie within a gap in the Fe bands. As can be seen in Table II, the peak widths increase with binding energy, as is generally accepted based on Auger lifetime-broadening arguments. Consistent with earlier studies, the $p_{x\pm y}$ minority-spin states exhibit less lifetime broadening than the majority-spin states at $\overline{\Gamma}$ as a result of the lower minority-spin-band occupancy. Hybridization with the Fe $3d$ bands introduces a pro-

nounced $k_\parallel$ dependence in both the linewidths and exchange splitting of the p_z orbitals. Both are larger at the zone center than at the zone edges. This results may be attributed to a variation in the amount of mixing with the d states across the zone.

The resonance features in the majority and minority bands at $\overline{\Gamma}$ exhibit the same binding energies as the corresponding features at the bulk Fe(001) surface, although the resonances in the film system are not as strong (compare Fig. 3 of Ref. 5 to Fig. 9 of this work). No independent angle-revolved data is available for comparison with our O resonance data along $\overline{\Gamma}$-$\overline{M}$; Panzner, Mueller, and Rhodin did not publish clean Fe(001) surface data with their $p(1\times1)$ O/Fe(001) data.[8] Figure 11, however, shows that the $\overline{\Gamma}$-$\overline{M}$ resonances exist near, if not coincident with, the location of a prominent clean-film majority band as mapped with spin-resolved photoemission.[13] The resonance band of Fig. 9 as determined from our angle-resolved data is therefore of majority-spin type except perhaps near the zone edge. The main resonance along $\overline{\Gamma}$-$\overline{X}$ is, upon comparison to the data of Clarke et al.,[5] also of majority-spin character. The film's resonance band in this symmetry direction lies at slightly lower binding energy than the bulk resonance band. No two-dimensional Fe band from the angle-resolved data is clearly degenerate with this resonance. However, the point $\overline{\Gamma}$ from the spin-resolved data suggests that (as can be seen in Fig. 11) the Fe bands in this region were simply

not clearly discernible in the angle-resolved data along $\bar{\Gamma}$-$\bar{X}$ (the same is true along $\bar{\Gamma}$-$\bar{M}$). The dispersion of the resonances on the film along $\bar{\Gamma}$-$\bar{X}$ (0.3 eV) is considerably smaller than that of the O resonance bands on bulk Fe (0.8 eV). We can attribute this to the two-dimensional nature of the Fe bands in the thin film since these bands are generally flatter than the corresponding Fe(001) bands.

V. CONCLUSION

We have reported a thorough spin-polarized photoemission study of adsorbate bands on an ultrathin ferromagnetic film. In addition, by using a W(001) crystal substrate, we were able to probe the exchange-split adsorbate bands along a symmetry direction impossible to access with bulk samples. Despite the large negative pressures exerted by epitaxying onto a W(001) substrate, the thin-film system has permitted us to measure the exchange-split adsorbate bands at $\bar{\Gamma}$ and $\bar{M}$. This tech-

nique opens up the possibility of studying chemical effects on magnetic surfaces which are excluded by use of bulk single-crystal magnetic surface. The marked similarities of the dispersions, exchange splittings, and linewidths obtained from the ultrathin-film system and the surface of the bulk are very encouraging and suggest that thin-film systems, which are frequently easier to maintain in a single-domain state than bulk crystals, may be the ideal configuration for studying magnetically interacting adsorbates.

[1]A. Liebsch, Phys. Rev. Lett. **38**, 248 (1977).

[2]A. Liebsch, Phys. Rev. B **27**, 1653 (1978).

[3]H. Huang and J. Hermanson, Phys. Rev. B **32**, 6312 (1985).

[4]P. D. Johnson, A. Clarke, N. B. Brookes, S. L. Hulbert, B. Sinkovic, and N. V. Smith, Phys. Rev. Lett. **61**, 2257 (1988).

[5]A. Clarke, N. B. Brookes, P. D. Johnson, M. Weinert, B. Sinkovic, and N. V. Smith, Phys. Rev. B **41**, 9659 (1990).

[6]B. Sinkovic, P. D. Johnson, N. B. Brookes, A. Clarke, and. N. V. Smith, Phys. Rev. Lett. **62**, 2740 (1989).

[7]R. A. DiDio, E. W. Plummer, and W. R. Graham, Phys. Rev. Lett. **52**, 683 (1984).

[8]G. Panzner, D. R. Mueller, and T. N. Rhodin, Phys. Rev. B **32**, 3472 (1985).

[9]G. Schönheuse, M. Donath, U. Kolac, and V. Dose, Surf. Sci. **206**, L888 (1988).

[10]H. Li, Y. S. Li, J. Quinn, D. Tian, J. Sokolov, F. Jona, and P. M. Marcus, Phys. Rev. B **42**, 9195 (1990).

[11]J. Chen and J. L. Erskine (unpublished).

[12]P. D. Johnson, S. L. Hulbert, R. Klaffky, N. B. Brookes, A. Clarke, B. Sinkovic, M. J. Kelley, and N. V. Smith (unpublished).

[13]R. L. Fink, G. A. Mulhollan, A. B. Andrews, J. L. Erskine, and G. K. Walters, J. Appl. Phys. **69**, 4986 (1991); A. B. Andrews, R. L. Fink, G. A. Mulhollan, J. L. Erskine, and G. K. Walters (unpublished).

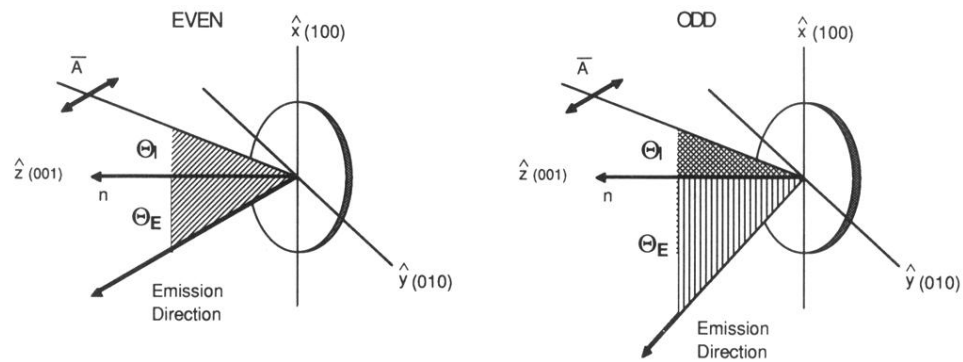[14]R. Wu and A. J. Freeman (private communication).

FIG. 1. Experimental geometry used in angle-resolved measurements. Light is incident on the sample at an angle θ_I with respect to the surface normal **n**. Electrons emitted at an angle θ_E with respect to the surface normal are collected by the analyzer. The light polarization and angle of incidence are set by rotating the sample about either the **x** or **y** axis. While electrons in both the even- and odd-state geometries are collected in a mirror plane containing the surface normal, the two geometries differ in that the vector potential **A** is parallel to the mirror plane in the even-state geometry and perpendicular to the mirror plane in the odd-state geometry.

p(1x1) Fe / W(100)

Real Space   Reciprocal Space

3.16Å

W surface atoms   ○
First-layer Fe atoms   ●
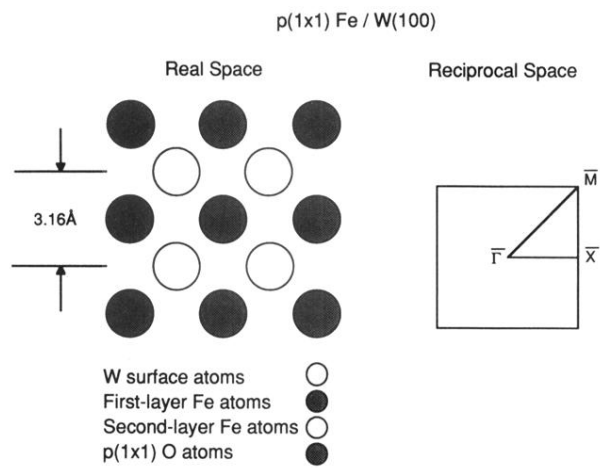Second-layer Fe atoms ○
p(1x1) O atoms   ●

FIG. 2. Real-space structure of $p(1 \times 1)$ O on 2 ML Fe/W(001) and corresponding two-dimensional Brillouin zone. The real-space structure is a view along the surface normal. Atoms of a given shading lie directly below other atoms denoted with the same shading, irrespective of species. Angle-resolved photoemission data were acquired along both in-plane high-symmetry directions with the in-plane momentum $k_{\parallel} = 0.512 (E_k)^{1/2} \sin\theta_E$ ranging from $\overline{\Gamma}\text{-}\overline{X}$ (along $\langle 100 \rangle$) and $\overline{\Gamma}\text{-}\overline{M}$ (along $\langle 110 \rangle$).